RSC Advances

1

Synthesis and characterization of Chitosan/montmorillonite/ZrO$_2$ nanocomposite and its application as adsorbent for removal of fluoride

Abbas Teimouri[a,*], Shima Ghanavati nasab[a], Saeed Habibollahi[a], Mahmoud Fazel-Najafabadi[b], Alireza Najafi Chermahini[c]

[a] *Chemistry Department, Payame Noor University, 19395-3697, Tehran, I. R. of Iran*
[b] *Mechanical Engineering Department, Payame Noor University, 19395-3697, Tehran, I. R. of Iran*
[c] *Department of Materials Engineering, Isfahan University of Technology, Isfahan 84156-83111, Iran*

ABSTRACT

A series of chitosan/montmorillonite/zirconium oxide (CTS/MMT/ZrO$_2$) nanocomposites were made by varying the molar ratios of chitosan (CTS) to montmorillonite/zirconium oxide (MMT/ZrO$_2$). The nanocomposites were characterized by FTIR, XRD and SEM. The surface area, pore volume and the pore size distribution of the CTS/MMT/ZrO$_2$ were calculated by BET technique. The effects of various molar ratios of CTS to MMT/ZrO$_2$, the initial pH value of the fluoride solution, contact time, temperature on adsorption capacities of samples for fluoride, adsorbent dose and initial concentration of fluoride were also investigated. The optimal conditions for removal of fluoride were found to be: molar ratio of CTS/MMT/ZrO$_2$, 1:1; pH: 4; temperature: 30 °C for 60 min in 25.00 mL of 20 mg/L of fluoride solutions and 0.1 gr of adsorbent. The fluoride adsorption capacity of CTS/MMT/ZrO$_2$ was also found to be 23 mg/g experimentally. The adsorption capacities of CTS, MMT, ZrO$_2$, CTS/ZrO$_2$, CTS/MMT and CTS/MMT/ZrO$_2$ nanocomposites, for fluoride removal were compared. The results indicated that the adsorption capacity of CTS/MMT/ZrO$_2$ nanocomposite was higher than the average values of those of CTS (52 mg/kg for fluoride removal), MMT, ZrO$_2$,

---

[*]Corresponding author at: Department of Chemistry, Payame Noor University (PNU), Isfahan, P.O. Box 81395-671, Iran. Tel.: +98 31 33521804; fax: +98 31 33521802.
E-mail addresses: a_teimouri@pnu.ac.ir, a_teimoory@yahoo.com (A. Teimouri).

2

CTS/ZrO$_2$ and CTS/MMT. The adsorption kinetics and isotherms were also examined. It was found that all the sorption processes were better described by pseudo-second-order equation and the Langmuir equation.

Keywords: Removal, Fluoride, Chitosan, Montmorillonite, Nano ZrO$_2$, Water, Adsorbent, Nanocomposite

Introduction

Fluoride is a necessary element, required for the maintenance of good dental health. Notwithstanding, fluoride concentrations in drinking water above 1.5 mg L^{-1} have been proved to have a detrimental effect on human health, leading to dental or skeletal fluoroses such as osteoporosis, arthritis and brittle bones.[1,2] Other deleterious effects include cancer, infertility, brain damage, Alzheimer syndrome and thyroid disorder. The World Health Organization (WHO) has set an acceptable and allowable limit range between 0.5 and 1.0 mg L^{-1} in drinking water.[1] It has however been estimated that more than 20 million people worldwide rely on drinking water with fluoride concentrations that surpass the WHO plumb line of 1.5 mg L^{-1}. One of the various ways by which fluoride toxicity may occur is, by acting positionally on the intestinal mucosa after ingestion. It then subsequently leads to the production of hydrofluoric acid in the venter, which leads to gastrointestinal annoyance or infectious results.[1] To remove fluoride from water, several physical, chemical and physico-chemical such as adsorption, ion exchange, precipitation, electro-dialysis and reverse osmosis have been developed.[3] Ion-exchange can eliminate fluoride up to 90–95%, but however, its disadvantage lies in its dependence on the use of resins, the modification of which still remains a challenging problem. Adsorption[3] has been reported to be one of the most efficient, economic and environment friendly for elimination of heavy metals from water and wastewater[4-7] among different defluoridation methods. A great number of materials have been studied, including impregnated and activated alumina,[8,9] rare earth oxides,[10] clays and other

3

soil materials,[11] impregnated silica,[12] carbon materials,[13,14] calcium-based materials,[15,16] bone

char,[17] fried egg jellyfish,[18] flower-like γ-AlOOH hierarchical superstructure,[19] amorphous

carbon nanotubes,[20] akaganéite (β-FeOOH) nanorods,[21] zeolites,[22] and natural biomaterials

like Chitosan-based adsorbents.[23,24] But, when the concentration of fluoride in water is

decreased to actual concentrations present in groundwater, generally below 10 mg/L, many of

these materials typically miss their defluoridation capacity.[25] In recent years, among the

various groups of adsorbents, biosorption has been identified as an efficient procedure for the

removal of metals in water and industrial sewages.[26] Chitosan is well established as a great

natural adsorbent because its amine (–NH$_2$) and hydroxyl (–OH) groups may serve as

coordination sites to form complexes with different metal ions. However, due to its solubility

in most dilute mineral acids, it is necessary to boost its chemical resistance through treatments

using crosslinking agents for application in acidic media. The crosslinking procedure may be

carried out by the reaction of Chitosan with several agents such as glutaraldehyde (GLA)

which additionally help to improve the adsorption capacity.[27] Also, Polymer/layered silicate

nanocomposites frequently exhibit remarkably significantly modified mechanical and material

properties and are attracting remarkable interest in the polymer science field.[28]

Montmorillonite is a kind of natural 2:1 type layered clay mineral with high cation exchange

capacity, swelling ability and high surface area.[29] Wang et al. prepared

Chitosan/montmorillonite (CTS/MMT) nanocomposites and discovered that the flocculated–

intercalated nanostructure was obtained at high MMT content while the intercalated exfoliated

nanostructure tended to form at low MMT content.[30] Darder et al. were also able to prepare

CTS/MMT nanocomposites and incorporate them in potentiometric sensors for use as anion

detectors.[31-33] Zirconia (ZrO$_2$) is a chemically inert inorganic metal oxide with high stability

toward acids, alkalis, oxidant and reductants.[34,35] The expectation is that its physical strength

and chemical inertness will increase the properties of chitosan upon formation of the

4

ZrO$_2$/chitosan composite. Additionally, its biocompatibility will contribute to the biocompatibility of the composite besides that of chitosan.[36] So for this research, we were able to successfully synthesize a kind of nanocomposite that is completely biocompatible. In the present study, a series of CTS/MMT/ZrO$_2$ nanocomposites were synthesized and characterized, and the adsorption kinetics and isotherms for fluoride (F$^-$) onto nanocomposite with CTS to MMT/ ZrO$_2$ were studied. The effects of various experimental conditions, such as different molar ratios of CTS to MMT/ZrO$_2$, the initial pH value of the fluoride solution, contact time, adsorbent dose and adsorption temperature were investigated.

Experimental section

Materials and Instruments

Chitosan and glutaraldehyde were purchased from Sigma-Aldrich. The degree of deacetylation and viscosity–average molecular weight of CTS are 85% and 9.0×10^5, respectively. Montmorillonite was obtained from Aldrich. Zirconium oxide nano powder was purchased from China Changsha Zhonglong Chemical (Group) Co., Ltd. Other agents used were all analytical grade and all solutions were prepared with distilled water. The samples were analyzed by X-ray diffraction (XRD) using a Philips X'PERT MPD X-ray diffractometer (XRD) with Cu K$_\alpha$ (1.5405 A$^\circ$). Data sets were prepared over the range of 5°–90° with a step size of 0.02° and a count rate of 3.0°/min. The structural morphology of the samples was analyzed using a scanning electron microscope (SEM, JEOL, JSM-6300, Tokyo, Japan). A JASCO FT/IR-680 PLUS spectrometer was used to record IR spectra using KBr pellets. The BET specific surface areas and BJH pore size distribution of the samples were determined by adsorption–desorption of nitrogen at liquid nitrogen temperature using a Series BEL SORP 18. The concentration of fluoride solutions were measured using a fluoride ion selective

5

electrode (Sartorius-PYI01) with the relative accuracy of ±1 significant digit, detection limit

of 0.05 mg/L using a TISAB buffer.

Adsorbent preparation

The Chitosan/Montmorillonite/ZrO$_2$ nanocomposite was prepared by the procedure of Wang

et al.[30] 2% ($\frac{W}{V}$) CTS solution (containing CTS amounts of 0.0660, 0.132, 0.660, 3.30, 6.60 g)

was prepared by dissolving CTS in 1% ($\frac{V}{V}$) aqueous acetic acid solution. The CTS solution

was then added to MMT/ZrO$_2$ (amount of MMT is twice of ZrO$_2$) mixture suspension in 50

$^\circ$C for 5 h to obtain the nanocomposites. The molar ratios of CTS to MMT/ ZrO$_2$ in the

nanocomposites were varied by using ratios of 1:10, 1:5, 1:1, 5:1 and 10:1, respectively to

obtain the series of nanocomposites. After 1 h, 25% ($\frac{V}{V}$) glutaraldehyde was added to the

mixture in a 1:40 volume ratio and stirred for another 1 h at 60 $^\circ$C. The composites were

neutralized with distilled water and the unreacted glutaraldehyde was eliminated. The

nanocomposite was then dried in the oven at 60 $^\circ$C for 12 h after which it was pulverized.

Adsorption experiments

The composites were prepared by applying batch experiments on a thermostated shaker. The

influence of the molar ratios of CTS to MMT/ZrO$_2$ on fluoride removal was carried out by

soaking 0.1 g of the adsorbent in 25.00 mL of fluoride solutions (20 mg/L, initial pH 7) at 30

$^\circ$C for 60 min, respectively. The effect of pH on fluoride removal was investigated by

immersing 0.1 g of the adsorbent in 25.00 mL of 20 mg/L fluoride solutions at 30 $^\circ$C for 60

min in different pH values (4.0, 5.0, 6.0, 7.0, 8.0 and 9.0). The influence of temperature on

fluoride removal was studied by immersing 0.1 g of adsorbent in 25.00 mL of solutions (20

mg/L, pH 4.0) at 30 $^\circ$C, 40 $^\circ$C and 50 $^\circ$C. The effect of adsorbent dose on fluoride removal was

also examined in 25.00 mL of solution (20 mg/L, pH 4.0) at 30 $^\circ$C for 60 min in adsorbent

6

doses (0.02, 0.04, 0.06, 0.08, 0.1, 0.12, 0.14, 0.16 and 0.18). The kinetics of fluoride

adsorption onto the synthesized nanocomposite was studied by adding 0.1 g of the

nanocomposite to 25.00 mL of fluoride solutions (20 mg/L, pH 4.0) at 30 °C. Also for

investigating the isotherm, 20 mg/L fluoride solutions (25.00 mL, pH 4.0) were shaken with

0.1 g of the adsorbent at 30 °C for 60 min.

The capacity of adsorbed fluoride (mg/g) was calculated according to the following

equation (1):

$$q_e = (C_0 - C_e)\frac{V}{m} \tag{1}$$

Where C_o and C_e are the initial and equilibrium concentrations of adsorbate (mg/L),

respectively, m is the mass of the adsorbent (g) and V is volume of the solution (L).

Statistical analysis

The collected data of percentages of the removal of fluoride were analyzed with one-way

analysis of variance (ANOVA) using SPSS software. Significant differences between

treatments were detected using the Tukey HSD test. The level of significance was

predetermined based on a probability of $p<0.05$.

Results and discussion

FT-IR analysis

The FTIR spectrum for CTS, MMT, ZrO_2 and CTS/MMT/ZrO_2 nanocomposite is reported in

the range, 400-4000 cm^{-1} in Fig. 1. The IR spectra of pure MMT as shown in Fig. 1 had the

band at 3635 cm^{-1} which was assigned to the structural hydroxyl group vibration.

Additionally, the bands at 1650 and 3442 cm^{-1} were attributed to the bending and stretching

vibrational modes of the hydrated O-H, respectively. The additional band seen in MMT at

1010 cm^{-1} was assigned to the Si-O bond. The IR spectra of the pure CTS showed the typical

band at 3363 cm^{-1} which was attributed to the stretching vibrations of the OH and N-H bonds.

7

Additionally, the band at 1653 cm^{-1} was assigned to the C=O bond of the acetyl group and while the band at 1070 cm^{-1} was assigned to C-O-C bond. The FTIR spectra of ZrO$_2$ showed an important band at 542 cm^{-1} corresponding to the vibration of the Zr-O bond. From Fig. 1. b, the bands in CTS (O–H and N–H stretching) which can be seen to overlap with the bands of MMT (–OH is stretching of H$_2$O) at 3424 cm^{-1} in addition to the band around 542 cm^{-1} related to ZrO$_2$ were all seen in the IR spectra of the nanocomposite.

As seen in Fig. 2, the intensity of the bands attached to the intercalated CTS (methylene (2882 cm^{-1}) groups and (C–H stretching on methyl (2923 cm^{-1}) and (C–H bending on methyl (1424 cm^{-1}) and methylene (1380 cm^{-1}) groups) in the spectra of the nanocomposites, increased with corresponding increase in the molar ratio of CTS to MMT/ZrO$_2$. Furthermore, the band at 1630 cm^{-1} became stronger with increasing molar ratios of MMT which was an indication that the first NH–CO group stretching vibration of CTS overlapped with the –OH bending vibration of H$_2$O in the MMT.[35]
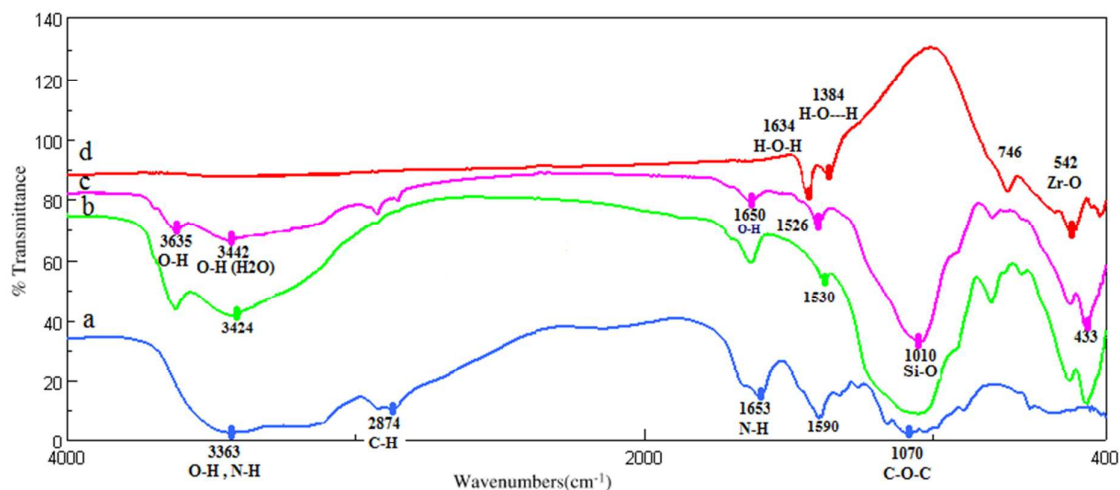
Fig. 1. FTIR spectra of the a) CTS; b) nanocomposites with the molar ratio of CTS to MMT/ZrO$_2$ 1:1; c) MMT; d) ZrO$_2$.

8
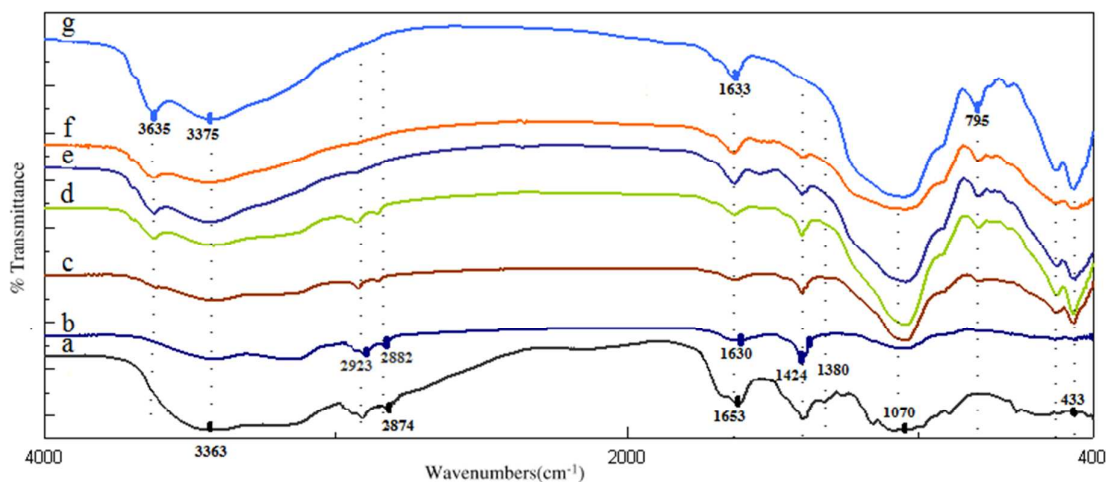
Fig. 2. FTIR spectra of the a) CTS; the nanocomposites with the molar ratios CTS to MMT/ZrO$_2$ of b) 10:1; c) 5:1; d) 1:1; e) 1:5; f) 1:10; g) MMT.

XRD analysis

X-ray diffraction (XRD) patterns of the adsorbent were obtained using Cu K$_\alpha$ radiation (λ=1.5405 A$^\circ$). The crystallite size of the crystalline phase was determined from the peak of maximum intensity by using Scherrer formula,[37] with a shape factor (K) of 0.9, which can be described as: Crystallite size=K.λ/W.cosθ, where W=W$_b$−W$_s$ while W$_b$ is the broadened profile width of experimental sample and W$_s$ the standard profile width of reference silicon sample.

As seen in Fig 3A, pure MMT typically displayed a diffraction peak at 6.94° whereas for CTS, the maximum was seen at 19°. In the XRD of ZrO$_2$, the sharp lines at 30.4, 51.0 and 60.2° were assigned to its tetragonal phase. However, in Fig 3B, a pattern can be observed from the top to the bottom, in which a gradual decrease of the MMT peak at 6.94° was seen as the amount used reduced. It can thus be stated that the formation of the flocculated structure in nanocomposites is due to the hydroxylated edge–edge interaction of the silicate layers. Furthermore, the reduction in the intensity of the peak with increasing molar ratios of CTS to CTS/ZrO$_2$ confirmed the formation of an intercalated–exfoliated structure in CTS/MMT/ZrO$_2$

9

nanocomposites. As a result, when CTS intercalated into MMT interlayer, it ruined the

crystalline structure of MMT.[35]
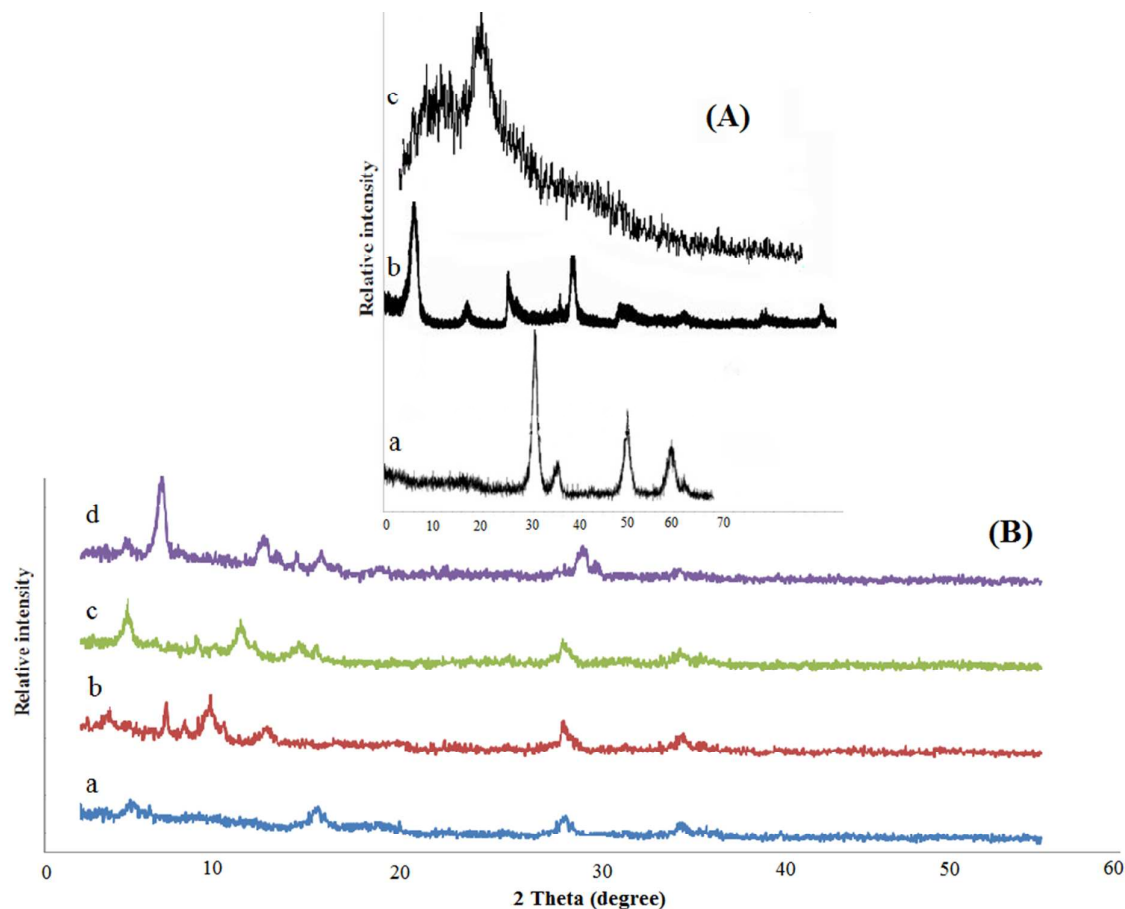
Fig. 3 (A)- XRD patterns of a) ZrO_2; b) MMT; c) CTS. (B)- XRD patterns of CTS/MMT/ZrO_2 nanocomposite with different molar ratio: a) 5:1; b) 1:1; c) 1:5; d) 1:10.

SEM analysis

SEM is a widely used technique for studying the morphology and surface characteristics of

adsorbents. In this study, SEM was used to detect any morphological changes in

CTS/MMT/ZrO_2 nanocomposite surface after synthesis. Fig. 4 shows the SEM images of CTS

(a), MMT (b), ZrO_2 (c), CTS/MMT/ZrO_2 nanocomposite before adsorption (d) and after

adsorption (e). Chitosan due to its wide surface, can act as a bed/support for MMT and ZrO_2.

From fig (d), MMT and ZrO_2 can be seen to be scattered on the surface of CTS. The SEM

10

images, show that the formation of adsorbent was successful and corroborate both the FT-IR

and XRD analysis results. Fig. 4 also showed the SEM images of the nanocomposite before

and after fluoride adsorption. Compared with the nanocomposite before sorption (Fig. 4d), the

fluoride-sorbed nanocomposite (Fig. 4e) does not possess any well-defined porous structure

and presented less prominent grooves.

a

b

c

11
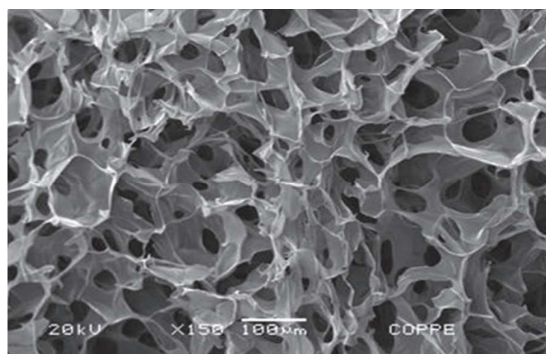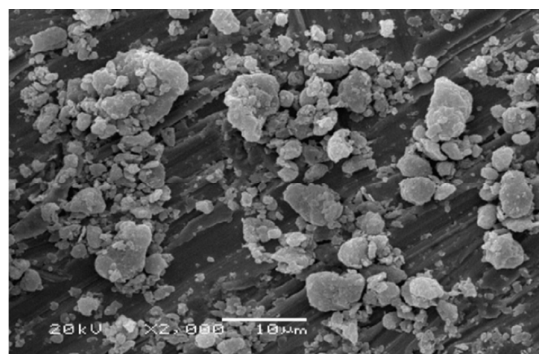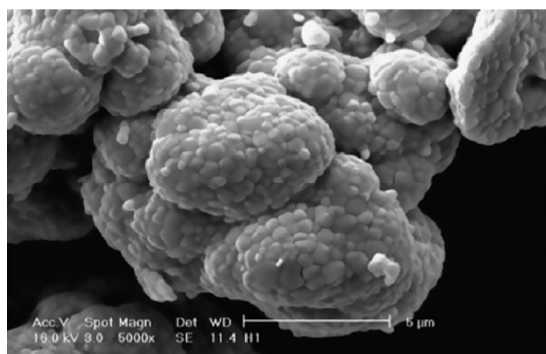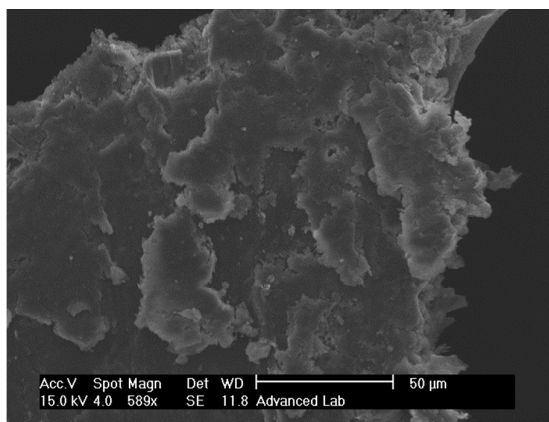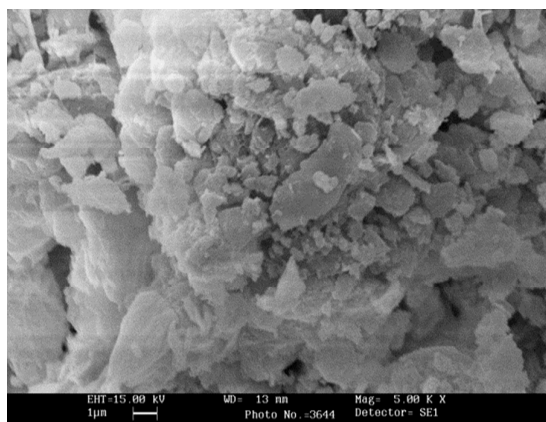
d   **e**

Fig. 4. SEM images of a) CTS; b) MMT; c) ZrO_2; d) nanocomposite before adsorption and e) after fluoride adsorption

BET Analysis

Table 1 gives the BET surface area values of the nanocomposite. The BET surface area, pore volume and average pore diameter are 62.448 m^2g^{-1}, 0.68 $cm^3\ g^{-1}$ and 0.923 nm respectively. The surface area of the nanocomposite was greater than that of pure CTS, most likely a result of the fact that the particles of MMT and ZrO_2, which possess high surface area, were scattered on the CTS bed and enlarged its surface. Consequently, since the average pore diameter of nanocomposite is larger than the diameter of fluoride ions, with 0.238 nm diameter, the anions were able to gain easy access into the pores. The sample was also mesoporous with N_2 adsorption–desorption isotherms of type IV with a H_3 hysteresis loop according to IUPAC classification. The Type H_3 loop, which does not display any limiting adsorption at high p/p°, is typically seen with aggregates of plate-like particles giving rise to slit-shaped pores.[40]

Table 1 BET surface area values of CTS/MMT/ZrO_2.

Nanocomposite	BET surface area (m^2g^{-1})	Pore volume ($cm^3\ g^{-1}$)	Average pore diameter (nm)
CTS/MMT/ZrO_2	62.448	0.68	0.923

Effect of molar ratios of CTS to MMT/ZrO_2 of nanocomposites on adsorption

Fig. 5, shows the effect of molar ratios of CTS to MMT/ZrO_2 on the fluoride adsorption capacity of the nanocomposites. As seen from Fig. 5, the fluoride adsorption capacities show corresponding increase with increasing molar ratios of CTS to MMT/ZrO_2. However, as the molar ratio of CTS to MMT/ZrO_2 approaches 1:1, a saturation point is reached beyond which the adsorption capacities only increase slightly. An explanation for this is that, the added CTS

12

serve to counter the initial negative charges of MMT while simultaneously increasing the fluoride adsorption capacities in the nanocomposites. As such, the fluoride adsorption capacities rapidly increase with increasing molar ratio of CTS to MMT/ZrO_2 from 1:10 to 1:1. However, since the amount of intercalated CTS is already saturated, there is only a slight increase in the adsorption capacities as the molar ratio of CTS to MMT/ZrO_2 exceeds 1:1.
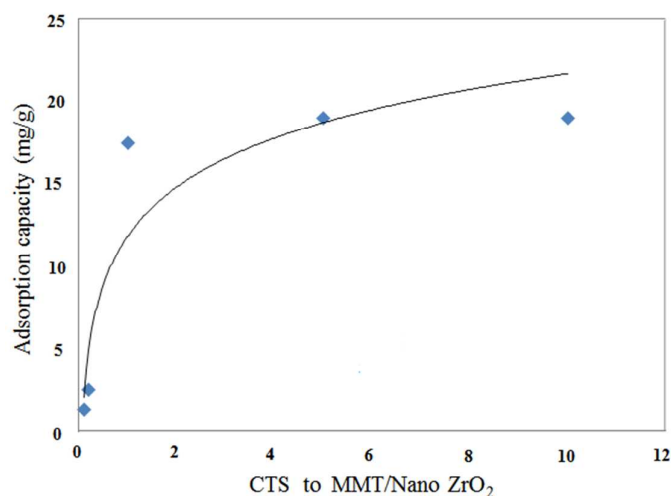
Fig. 5. Effect of the molar ratios of CTS to MMT/ZrO_2 on adsorption capacity of the nanocomposites for fluoride. Concentration: 20 mg/L; sample range: 0.1 g/25.00 mL; natural pH; temperature: 30 $^\circ$C; equilibrium time: 60 min.

Effect of pH value on adsorption

Another important factor affecting the adsorption capacity is the pH of the analyte solutions. The effect of the pH value of the standard solution on the fluoride adsorption capacity is displayed in Fig. 6. It can be clearly seen that when the pH value of the fluoride solution rose from 4 to 9, the adsorption capacity decreased from 22.50 to 2.50, 17.00 to 2.00 and 12.00 to 1.00 mg/g for CTS/MMT/ZrO_2 nanocomposite, CTS/ZrO_2 and CTS/ MMT, respectively. Furthermore, the adsorption capacity of CTS/MMT/ZrO_2 nanocomposite was seen to be higher than CTS/ZrO_2 and CTS/ MMT at all pH. Also, fluoride adsorption capacity of ZrO_2 is 19 mg/g[38] and fluoride adsorption capacity for MMT is 0.263 mg/g.[39]

13
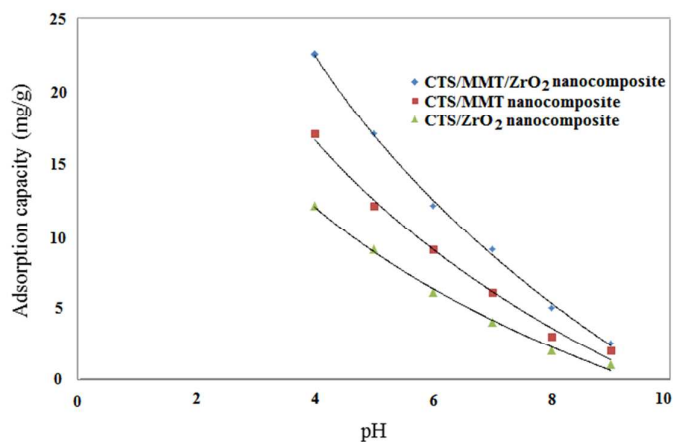
Fig. 6. Effect of the pH values on adsorption capacity of CTS/ZrO$_2$, CTS/MMT and the CTS/MMT/ZrO$_2$ nanocomposite for fluoride. Fluoride concentration: 20 mg/L; sample range: 0.1 g/25.00 mL; pH range: 4–9; temperature: 30 $^{\circ}$C; equilibrium time: 60 min.

Effect of temperature on adsorption

The relationship between the temperature and the fluoride adsorption capacity of the adsorbent is shown in Fig. 7. The adsorption capacity of the adsorbent increased from 22.50 to 25.00 with increasing temperatures from 30 to 50 $^{\circ}$C. It can thus be concluded that the adsorption process is an endothermic one. However, as it is not economical to operate at elevated temperatures 30 $^{\circ}$C was chosen as the optimal temperature.
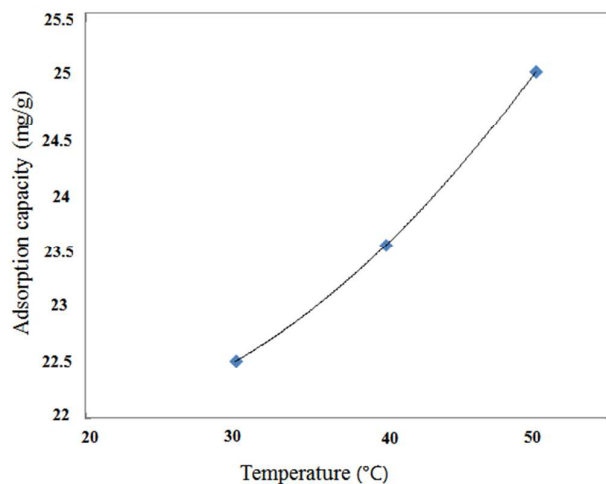
Fig. 7. Effect of the temperature on adsorption capacity of the CTS/MMT/ZrO$_2$ nanocompositefor fluoride. Fluoride concentration: 20 mg/L; sample range: 0.1 g/25.00 mL; pH: 4; temperature: 30–50 $^{\circ}$C; equilibrium time: 60 min.

14

Effect of adsorbent dose on adsorption

Effect of adsorbent dose on fluoride removal at fluoride concentration of 20 mg/L, pH 4 and temperature 30 $^{\circ}$C is shown in Fig. 8. It was shown that percentage removal of fluoride increased from 10% to 48.5% with an increase in adsorbent dose from 0.02 to 0.18 g/25.00 mL, respectively. This is due to the fact that with increasing of adsorbent dose, the surface area of adsorbent is increased. It was seen that after a dosage of 0.1 g, there was no noticeable change in the percentage removal of fluoride. Therefore, the optimum dose was chosen 0.1 g/25.00 mL.
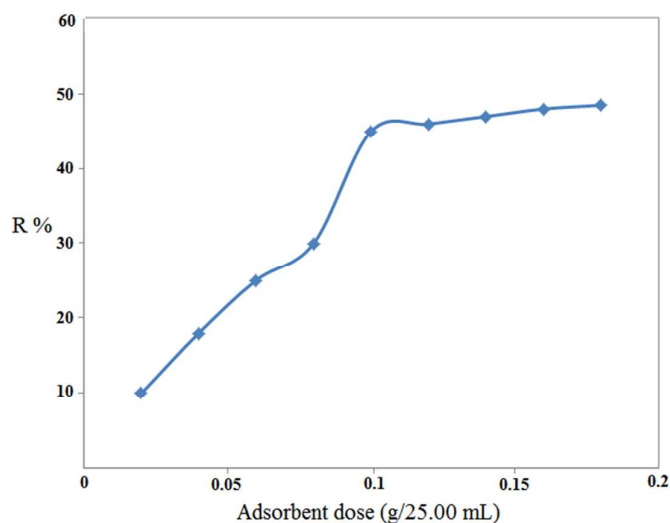
Fig. 8. Effect of adsorbent dose on the percentage removal of fluoride ion at fluoride concentration: 20 mg/L; pH: 4; temperature: 30 $^{\circ}$C; equilibrium time: 60 min.

Mechanism of fluoride adsorption

As shown in Scheme 1, a suitable mechanism for the removal of fluoride ion has been proposed. Two possible mechanisms of adsorption of fluoride by CTS/MMT/ZrO$_2$ composite may be considered: (a) electrostatic interaction between protonated amine groups (NH$_3^+$) groups of CTS and the fluoride ion may be adsorbed by the positive charge Zr^{2+} and Al^{3+}in the composite attracts negatively charged fluoride ions via electrostatic attraction. In this

15

mechanism interaction of fluoride ion with OH groups on the surface might occur.[41] (b)

complexation mechanism may also occur as fluoride acts as a chelating agent.[42]

CTS/MMT/ZrO$_2$ composite
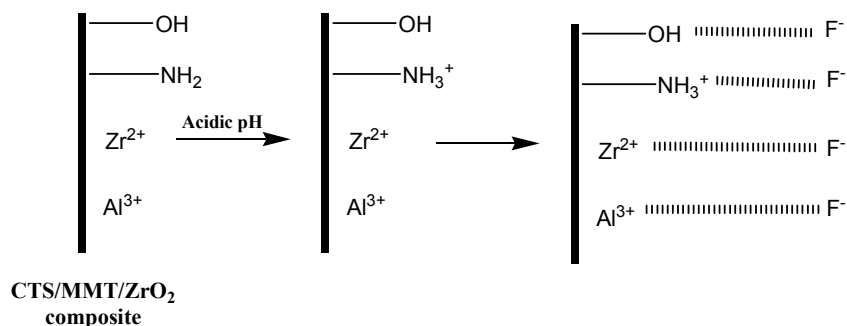
Scheme 1 Sorption mechanism between the adsorbent and fluoride ion.

Adsorption kinetics

The influence of contact time on adsorption capacity of fluoride by the CTS/MMT/ZrO$_2$

nanocomposite was studied. It was concluded that the adsorption capacity of nanocomposite

increased rapidly in the primary steps of contact time and then slowed as the contact time

increased until it attained equilibrium and the adsorption equilibrium of fluoride on the

nanocomposite was attained in 60 min. Therefore, for the test, an adsorption time of 60 min

was selected for the adsorption isotherms, to ensure that the adsorption equilibrium was

attained. Two simplified kinetic models containing pseudo-first-order and pseudo-second-

order equations were analyzed. A simple kinetic model that describes the process of

adsorption is the pseudo-first-order equation. It was suggested by Lagergren,[43] for the

adsorption of solid/liquid systems and its formula is given below as;

$$\frac{dq_e}{dt} = k_1 \left(q_e - q_t \right) \tag{2}$$

Where k$_1$ is the pseudo-first-order rate constant (min^{-1}), q$_e$ and q$_t$ are the amounts of

fluoride adsorbed (mg/g) at equilibrium and at time t (min). After integration with the initial

condition q$_t$ =0 at t = 0, Eq. (3) can be obtained:

16

$$\log(q_e - q_t) = \log q_e - \frac{k_1}{2.303}t \tag{3}$$

The pseudo-second-order model based on adsorption equilibrium capacity is given below as:[44]

$$\frac{dq_e}{dt} = k_2(q_e - q_t)^2 \tag{4}$$

When the initial condition is $q_t = 0$ at $t = 0$, integration leads to the following equation:

$$\frac{t}{q_t} = \frac{1}{k_2 q_e^2} + \frac{t}{q_e} \tag{5}$$

Where k_2 (g mg^{-1} min^{-1}) is the rate constant of the pseudo-second-order adsorption. The linear plots of log (q_e-q_t) versus t and (t/q_t) versus t drawn for the pseudo-first-order and the pseudo-second-order models, respectively. The rate constants k_1 and k_2 can be obtained from the plot of experimental data. The regression coefficients R^2 of the pseudo first-order model is 0.9153 and for the pseudo-second-order model, it is 0.9847 in the 20 mg/L fluoride solution. This shows that the adsorption of fluoride on nanocomposite could be better described by the pseudo-second-order rather than by the pseudo-first-order. This result also shows that the adsorption rate of fluoride depends on the concentration of fluoride at the adsorbent surface and the absorption of these adsorbed at equilibrium.[45]

Table 2 Kinetic parameter for sorption of F$^-$ ion onto a CTS/MMT/ZrO$_2$ nanocomposite.

F$^-$	$q_{e(exp)}$ (mg/g)	Pseudo-first-order			Pseudo-second-order		
C_0 (mg/L)		$q_{e(cal)}$ (mg/g)	K_1 (1/min)	R^2	$q_{e(cal)}$ (mg/g)	K_2 (g/mg min)	R^2
10	20	41.68	0.0589	0.9102	21.30	0.1506	0.9950
15	22	50.27	0.0624	0.8976	22.8	0.1805	0.9901
20	23	52.42	0.0741	0.9153	24.50	0.2154	0.9847
30	23.40	66.72	0.0741	0.8803	24.82	0.2202	0.9880

Adsorption isotherms

The adsorption capacity of fluoride by nanocomposite at different fluoride concentrations and at 30 °C for samples was investigated. The results showed a sharp increase in adsorption

17

capacity as the fluoride concentration increased from 1 to 20 mg/L for the nanocomposite. This is an indication that the fluoride adsorption capacity of the nanocomposite was enhanced by increasing the fluoride concentration. However, increasing the initial concentration of fluoride beyond 20 mg/L only led to a slight increment in the adsorption capacity of the nanocomposite. The adsorption process can be commonly described by two isotherm equations, namely, the Langmuir and the Freundlich equations,[46] which are displayed by the following equations, respectively:

$$\frac{C_e}{q_e} = \frac{1}{bq_m} + \frac{C_e}{q_m} \tag{6}$$

$$q_e = k_f C_e^{1/n} \tag{7}$$

Where q_m (mg/g) and b (L/mg) are Langmuir isotherm coefficients. The value of q_m shows the maximum adsorption capacity. K_f (mg/g) and n are Freundlich constants. The linear plot of C_e/q_e versus C_e drawn for the Langmuir model of the adsorption of fluoride. The applicability of the Langmuir isotherm expressed the monolayer cover of the fluoride on the surface of nanocomposite. The linearization of the equations is y= 0.0404x+0.1155 and the values of R^2 for nanocomposite is 0.9991. The q_m value for the adsorption of fluoride by nanocomposite was 24.752 mg/g. The value of R^2 of Freundlich model for nanocomposite is 0.8523. So, the adsorption of fluoride on nanocomposite do not fit the Freundlich isotherm. Furthermore, a comparative evaluation of adsorption capacity (mg/g) and other experimental conditions of composites based on Chitosan for fluoride removal is shown in Table 4.

Table 3 Values of different isotherm parameters.

F⁻ sorption
Langmuir isotherm

18

q_m (mg/g)	24.752
b (L/mg)	0.3497
R^2	0.9991
Freundlich isotherm	
K_f	9.7903
1/n	0.2335
R^2	0.8523

Table 4 A comparative evaluations of adsorption capacity (mg/g) and other experimental conditions of composites based on Chitosan for fluoride removal.

Biosorbent	Experimental conditions	Amount adsorbed (mg/g)	References
Al-doping chitosan–Fe(III) hydrogel	pH: 5.0 Concentration: 10 mg/L Temperature: 25 °C	31.16	47
lanthanum incorporated chitosan beads	pH: 5.0 Concentration: 5.34 mg/L Temperature: 30 °C	4.7	48
lanthanum impregnated chitosan flakes	pH: 6.7 Concentration: 5 mg/L Temperature: n.a	1.27	49
La-incorporated chitosan beads	pH: n.a Concentration: 5.35 mg/L Temperature: 30 °C	4.7	50
chitosan supported zirconium(IV) tungstophosphate composite	pH: 3.0 Concentration: 10 mg/L Temperature: 30 °C	2.025	51
protonated cross-linked chitosan particles	pH: 7.0 Concentration: 10 mg/L Temperature: 30 °C	8.10	52
protonated chitosan beads	pH: 7.0 Concentration: 19 mg/L Temperature: 30 °C	1.664	53
protonated cum carboxylated chitosan beads	pH: 7.0 Concentration: 10 mg/L Temperature: 30 °C	1.8	54
CTS/MMT/ZrO$_2$ nanocomposite	pH: 4.0 Concentration: 20 mg/L Temperature: 30 °C	23	Present study

Interaction among the variables for percentage of fluoride removal

Fig. 9 (a, b and c) illustrates the interactive effect of three variables with respect to percentage removal. Fig. 9 (a) shows the interaction between molar ratio and temperature to percentage removal of fluoride. It correlates higher molar ratio above 1:1 and prolonged temperature

19

from 30 to 50 $^{\circ}$C with percentage removal. Higher temperature above 40 $^{\circ}$C increased percentage removal within 1:1 of molar ratio.

Fig. 9 (b) illustrates the relationship among molar ratio and pH on percentage removal. Increasing pH from 4 to 9 decreased percentage removal. Maximum percentage removal at about 45% (adsorption capacity= 23) was obtained at pH 4 and 5:1 molar ratio.

And finally, Fig. 9 (c) shows the influence of pH and temperature on percentage removal. Increasing temperatures from 30 to 50 $^{\circ}$C and reduction of pH from 9 to 4, increased percentage removal. Maximum percentage removal at about 45% was obtained at pH 4 and 50 $^{\circ}$C.
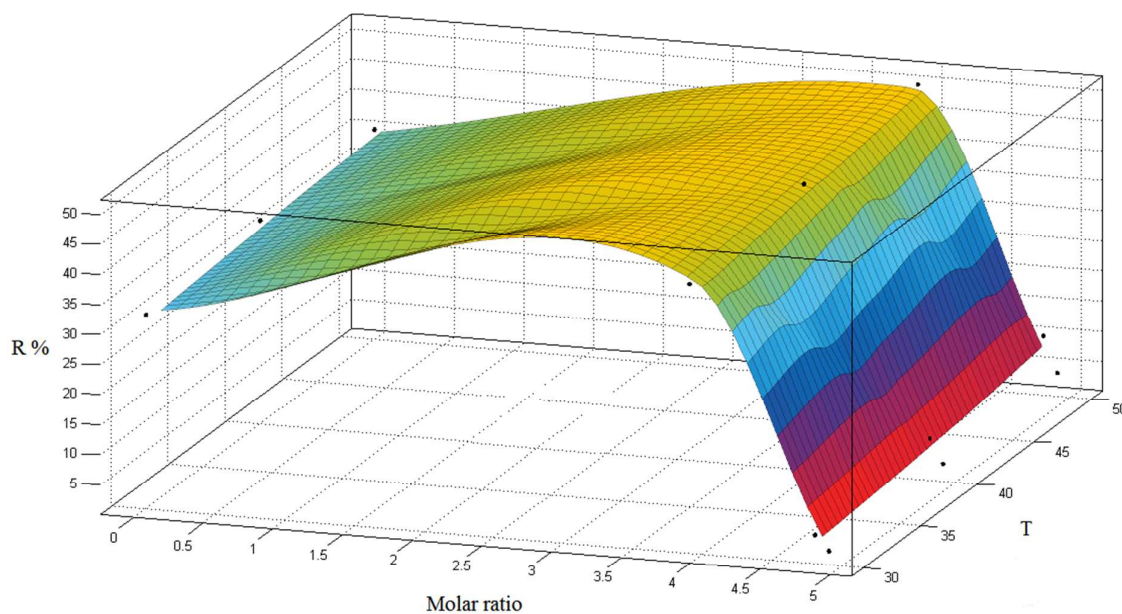
a

20
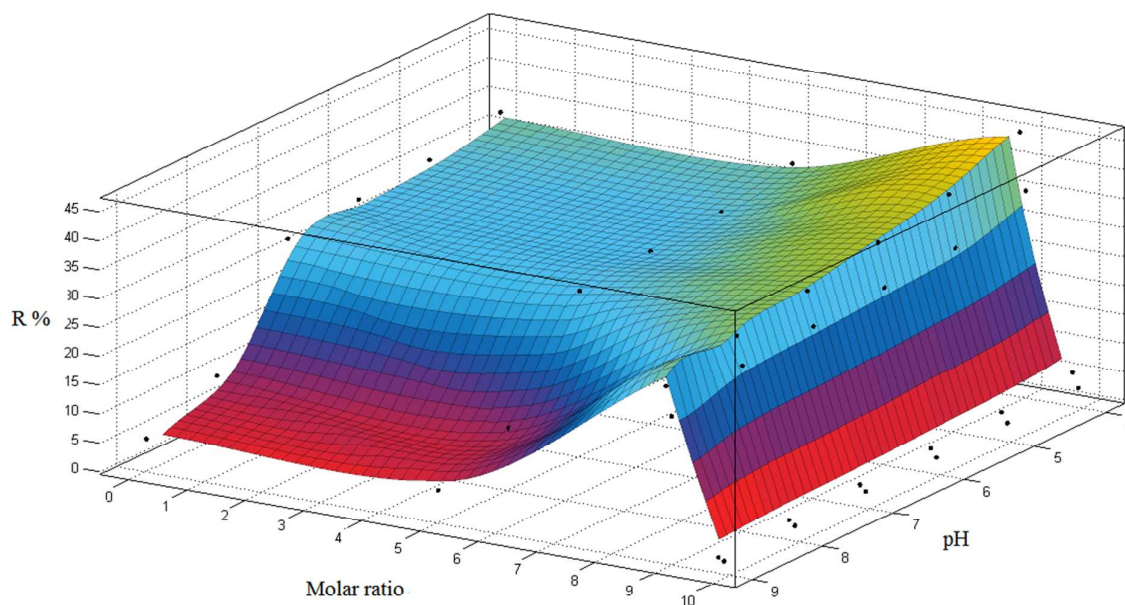
b
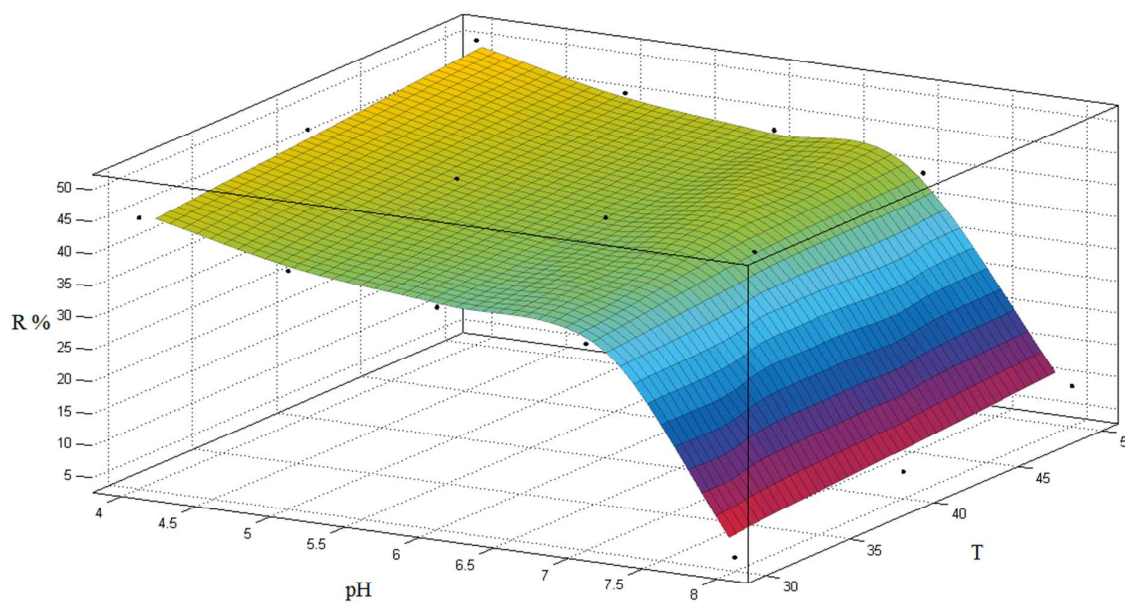
c

Fig. 9. Three dimensional contour plot for percentage removal (a) molar ratio and temperature; (b) molar ratio and pH; c) pH and temperature.

21

One of the most considerable advantages of adsorbents in operation is the possibility of reuse, without significant loss in sorption ability. The adsorbents were used in 6 runs and after each run, the adsorbent was separated by filtration, washed thrice with 5 ml NaOH (NaOH was used as desorption agent, because it aided the release of fluoride ions which where bonded to the amino groups on CTS chains allowing them to revert to initial state). It was subsequently washed with distilled water severally and dried in an oven at 60 $^\circ$C for about 8 h. The recovered adsorbent could then be reused in the next run. A comparison of the percentage removal in six sequential runs (45%, 41%, 38%, 35%, 30% and 28%) showed that the adsorbent could be reused several times.

Conclusions

In this study, a novel low-cost biosorbent, chitosan/montmorillonite/ZrO_2 nanocomposite material was prepared using environmentally friendly and cheap chitosan, clay and zirconium oxide. It could rapidly and efficiently remove fluoride under acidic conditions via the chelation between F$^-$ and amine group of complex. The results represent that the fluoride adsorption process is dependent on the molar ratios of CTS to MMT/ZrO_2, initial pH value of the fluoride solution, adsorbent dose and temperature. By varying these parameters optimal conditions for fluoride adsorption were obtained. The adsorption kinetics were seen to follow the pseudo-second-order model, and the isotherm obeyed the Langmuir monolayer model. Compared with CTS, MMT, ZrO_2, CTS/ZrO_2 and CTS/MMT, the CTS/MMT/ZrO_2 nanocomposite has higher adsorption capacity. So, the nanocomposite can be effectively used as an adsorbent for the removal of fluoride.

Conflict of interest
The authors declare no competing financial interest.

22

Acknowledgement

Notes and references

1 A. Bhatnagar, E. Kumar, M. Sillanpaa, Chemical Engineering Journal, 2011, 171, 811– 840.

2 P. Miretzky, A. F. Cirelli, Journal of Fluorine Chemistry, 2011, 132, 231–240.

3 A. Lal Srivastav, P. K. Singh, V. Srivastava, Y. C. Sharma, J. Hazardous Materials, 2013, 263, 342–352.

4 R.K. Gautam, S.K. Sharma, S. Mahiya, M.C. Chattopadhyaya, RSC, London, Chapter 1 2014 , 1-24.

5 R.K. Gautam, S.K. Sharma, M.C. Chattopadhyaya, RSC, London, Chapter 4, 2014, 57-85.

6 R.K. Gautam, A. Mudhoo, G. Lofrano, M.C. Chattopadhyaya, Journal of Environmental Chemical Engineering, 2014, 2, 239–259.

7 R.K. Gautam, A. Mudhoo and M.C. Chattopadhyaya, Journal of Environmental Chemical Engineering, 2013, 1, 1283–1291.

8 N. Das, P. Pattanaik, R. Das, J. Colloid Interface Sci., 2005, 292, 1–10.

9 D. Mohapatra, D. Mishra, S.P. Mishra, G.R. Chaudhury, R.P. Das, J. Colloid Interface Sci., 2004, 275, 355–359.

10 A.M. Raichur, J.M. Basu, Sep. Purif. Technol., 2001, 24, 121–127.

11 M. Agarwal, K. Rai, R. Shrivastav, S. Dass, J. Cleaner Prod., 2003, 11, 439–444.

12 S.A. Wasay, M.J. Haron, S. Tokunaga, Water Environ. Res., 1996, 68, 295–300.

13 I. Abe, S. Iwasaki, T. Tokimoto, N. Kawasaki, T. Nakamura, S. Tanada, J. Colloid Interface Sci., 2004, 275, 35–39.

23

14 Y.H. Li, S. Wang, X. Zhang, J. Wei, C. Xu, Z. Luan, D. Wu, B. Wei, Environ. Technol., 2003, 24, 391–398.

15 C.S. Sundaram, N. Viswanathan, S. Meenakshi, J. Hazard. Mater., 2008, 155, 206–215.

16 S. Gao, R. Sun, Z. Wei, H. Zhao, H. Li, F. Hua, J. Fluorine Chem., 2009, 130, 550–556.

17 S. Gao, J. Cui, Z. Wei, Study on the fluoride adsorption of various apatite materials in aqueous solution, J. Fluorine Chem., 2009, 130, 1035–1041.

18 Y. X. Zhang, X. Y. Yu, Z. Jin, Y. Jia, W. H. Xu, T. Luo, B. J. Zhu, J. H. Liu and X. J. Huang. J. Mater. Chem., 2011, 21, 16550–16557.

19 Y. X. Zhang, Y. Jia, Z. Jin, X. Y. Yu, W. H. Xu, T. Luo, B. J. Zhu, J. H. Liu and X. J. Huang. CrystEngComm, 2012, 14, 3005-3007.

20 Y. X. Zhang, Z. L. Liu, B. Sun, W. H. Xu and J. H. Liu. RSC.Adv., 2013, 3, 23197-23206.

21 Y. X. Zhang, Y. Jia. Appl. Surf. Sci., 2014, 290, 102-106.

22 M.S. Onyango, Y. Kojima, O. Aoyi, E.C. Bernardo, H. Matsuda, J. Coloid Interface Sci., 2004, 279, 341–350.

23 S. Jagtap, D. Thakre, S. Wanjari, S. Kamble, N. Labhsetwar, S. Rayalu, J. Colloid Interface Sci., 2009, 332, 280–290.

24 D. Mohan, R. Sharma, V.K. Singh, P. Steele, C.U. Pittman Jr., Ind. Eng. Chem. Res., 2012, 51, 900–914.

25 L. Gómez-Hortigüela, J. Pérez-Pariente, R. García, Y. Chebude, I. Díaz, Separation and Purification Technology, 2013, 120, 224–229.

26 M. Rajiv Gandhi, N. Viswanathan, S. Meenakshi, International Journal of Biological Macromolecules, 2010, 47, 146–154.

27 V. N. Tirtom, A. Dincer, S. Becerik, T. Aydemir, A. Celik, Chemical Engineering Journal, 2012, 197, 379–386.

28 G. Lagaly, Appl. Clay Sci., 1999, 15(1–2), 1–9.

24

29 D. Chen, W. Li, Y. Wu, Q. Zhu, Z. Lu, G. Du, Chemical Engineering Journal, 2013, 221, 8–15.

30 S.F. Wang, L. Shen, Y.J. Tong, L. Chen, I.Y. Phang, P.Q. Lim, T.X. Liu, Polym. Degrad. Stab., 2005, 90(1), 123–131.

31 M. Darder, M. Colilla, E. Ruiz-Hitzky, Chem. Mater., 2003, 15(20), 3774–3780.

32 M. Darder, M. Colilla, E. Ruiz-Hitzky, Appl. Clay Sci., 2005, 28(1–4), 199–208.

33 L.Wang, A.Wang, Journal of Hazardous Materials, 2007, 147, 979–985.

34 L. Kljajevi´c, B. Matovi´c, A. Radosavljevi´c-Mihajlovi´c, et al., Journal of Alloysand Compounds, 2011, 509, 2203–2215.

35 H.L. Liu, X.F. Sun, C.Q. Yin, C. Hu, Journal of Hazardous Materials, 2008, 151, 616–622.

36 H. Jiang, P. Chen, Sh. Luo, X. Tu, Q. Cao, M. Shu, Applied Surface Science, 2013, 284, 942–949.

37 B. D. Cullity and S. R. Stock, Elements of X-ray Diffraction, Prentice Hall, Upper Saddle River, NJ, 3rd edn, 2001, p. 388.

38 J.A. Blackwell, P.W. Carr, J. Chromatogr., 1991, 549, 43–57.

39 A. Tor, Desalination, 2006, 201, 267–276.

40 K. S. W. Sing, D. H. Everett, R. A. W. Haul, L. Moscou, R. A. Pierott, J. Rouquerol, T. Siemieniewska, Pure & Appl. Chem., 1985, 57, 603-619.

41 C. Namasivayam, D. Kavitha, Dyes Pigments, 2002, 54, 47–58.

42 N. Viswanathan, C.S. Sundaram, S. Meenakshi, J. Hazard. Mater, 2009, 167, 325–333.

43 S. Lagergren. Kungliga Svenska Vetenskapsakademiens Handlingar, 1898, 24, 1–39.

44 Y.S. Ho, G. McKay. Process Biochem., 1999, 34, 451–465.

45 S.L. Sun, A.Q. Wang. J. Hazard. Mater., 2006, 131, 103–111.

46 K. Periasamy, C. Namasivayam. Waste Manage., 1995, 15, 63–68.

25

47 J. Ma, Y. Shen, Ch. Shen, Y. Wen, W. Liu, Chemical Engineering Journal, 2014, 248, 98–106.

48 A. Bansiwal, D. Thakre, N. Labhshetwar, S. Meshram, S. Rayalu, Colloids and Surfaces B: Biointerfaces, 2009, 74, 216–224.

49 S. Jagtap, M. Kumar Yenkie, S. Das, S. Rayalu, Desalination, 2011, 273, 267–275.

50 D. Thakre, S. Jagtap, A. Bansiwal, N. Labhsetwar, S. Rayalu, Journal of Fluorine Chemistry, 2010, 131, 373–377.

51 N. Viswanathan, S. Meenakshi, Journal of Hazardous Materials, 2010, 176, 459–465.

52 R. Huang, B. Yang, Q. Liu, K. Ding, Journal of Fluorine Chemistry, 2012, 141, 29–34.

53 N. Viswanathan, C. S. Sundaram, S. Meenakshi, Journal of Hazardous Materials, 2009, 161, 423–430.